Original Research Article

Pulmonary Circulation

A computational model of contributors to pulmonary hypertensive disease: impacts of whole lung and focal disease distributions

Behdad Shaarbaf Ebrahimi[1], Merryn H. Tawhai[1], Haribalan Kumar[1], Kelly S. Burrowes[1], Eric A. Hoffman[2], Margaret L. Wilsher[3,4], David Milne[5] and Alys R. Clark[1]

[1]Auckland Bioengineering Institute, University of Auckland, Auckland, New Zealand; [2]Department of Radiology, University of Iowa, Iowa City, IA, USA; [3]Respiratory Services, Auckland City Hospital, Auckland, New Zealand; [4]Faculty of Medical and Health Sciences, University of Auckland, Auckland, New Zealand; [5]Department of Radiology, Auckland City Hospital, Auckland, New Zealand

Abstract

Pulmonary hypertension has multiple etiologies and so can be difficult to diagnose, prognose, and treat. Diagnosis is typically made via invasive hemodynamic measurements in the main pulmonary artery and is based on observed elevation of mean pulmonary artery pressure. This static mean pressure enables diagnosis, but does not easily allow assessment of the severity of pulmonary hypertension, nor the etiology of the disease, which may impact treatment. Assessment of the dynamic properties of pressure and flow data obtained from catheterization potentially allows more meaningful assessment of the strain on the right heart and may help to distinguish between disease phenotypes. However, mechanistic understanding of how the distribution of disease in the lung leading to pulmonary hypertension impacts the dynamics of blood flow in the main pulmonary artery and/or the pulmonary capillaries is lacking. We present a computational model of the pulmonary vasculature, parameterized to characteristic features of pulmonary arterial hypertension and chronic thromboembolic pulmonary hypertension to help understand how the two conditions differ in terms of pulmonary vascular response to disease. Our model incorporates key features known to contribute to pulmonary vascular function in health and disease, including anatomical structure and multiple contributions from gravity. The model suggests that dynamic measurements obtained from catheterization potentially distinguish between distal and proximal vasculopathy typical of pulmonary arterial hypertension and chronic thromboembolic pulmonary hypertension. However, the model suggests a non-linear relationship between these data and vascular structural changes typical of pulmonary arterial hypertension and chronic thromboembolic pulmonary hypertension which may impede analysis of these metrics to distinguish between cohorts.

Keywords

computational modeling, pulmonary hypertension, pulmonary circulation, vascular remodeling

Date received: 13 June 2021; accepted: 1 October 2021

Pulmonary Circulation 2021; 11(4) 1–15
DOI: 10.1177/20458940211056527

Introduction

Pulmonary hypertension (PH) is a pathology originating within the lung or heart that results in increased pulmonary blood pressures, putting strain on the right heart, which can ultimately lead to cor pulmonale. PH is typically diagnosed when mean pulmonary artery pressure (mPAP) exceeds 20 mmHg at rest,[1] sometimes in conjunction with elevated pulmonary capillary wedge pressure. These static measures are not considered to be predictive of the severity of PH.[2] It is the dynamic load on the right heart that ultimately determines the strain that it is under due to PH and the resultant severity.[3]

The underpinnings of elevated blood pressures in the pathophysiology of PH are complex and multi-factorial. Pulmonary arterial hypertension (PAH) and chronic

Corresponding author:
Alys R. Clark, Auckland Bioengineering Institute, University of Auckland, Private Bag 92019, Auckland 1142, New Zealand.
Email: alys.clark@auckland.ac.nz

thromboembolic pulmonary hypertension (CTEPH) are subtypes of PH that are defined by the presence of precapillary hypertension and degrees of small vessel arteriopathy.[4] CTEPH differs from PAH, as it is also associated with proximal occlusion of the pulmonary arteries which can cause significant alterations to perfusion and elevate pulmonary blood pressures beyond the level that would occur through vascular remodeling alone.[5–7] Diagnostic methods should, ideally, be able to distinguish these differences as well as between pathology of the micro- and macrovasculature in different forms of PH. In PAH, CTEPH, and other forms of PH, uncertainty in diagnosis can impact on treatment outcomes.[8] For example, pulmonary thromboendarterectomy (PTE) surgery is one of the most effective curative options for CTEPH patients.[9] Although this surgery is effective,[10] many patients still show signs of impaired pulmonary vascular function after removal of lesions. This implies an important effect of irreversible microvascular remodeling that persists in the distal arteries and cannot be removed by surgery.[11] Methods to distinguish between (reversible) thrombosis and (irreversible) remodeling of the vasculature will assist clinical decision making.

Mean pulmonary artery pressure or mPAP, despite being the most commonly used metric to confirm PH, does not effectively distinguish between PAH and CTEPH.[12] There is evidence to suggest that characteristics of the dynamic changes in pressure and flow waveforms at the main pulmonary artery (MPA) can enable a meaningful distinction between the two.[5,6] For example, characteristics of MPA impedance (the opposition of pulmonary vasculature to pulsatile flow) and wave reflection have been proposed to be early markers of PH severity,[5,6] and there is evidence that CTEPH patients show indications of increased wave reflection (due to proximal occlusions) compared to PAH patients.[5] Elevated wave reflection markers in CTEPH patients have been shown to persist even after pulmonary endarterectomy,[13] demonstrating the impact of vascular remodeling. Estimation of large vessel resistance has been used to assess the hemodynamic contributions of large and small vessels in CTEPH,[14] to enable assessment of the extent of small vessel disease post-PTE operation. These measurements provide a way to distinguish between these patients and hence have the potential to introduce a step change in current clinical practice.

Computational models are a valuable addition to the surgical armamentarium for assessment of CTEPH[15] and are useful in predicting system-level response to changes in pulmonary vascular physiology.[16,17] To confidently distinguish between micro- and macrovascular disease, models must incorporate function across the whole spatial scale range of the pulmonary vasculature. However, to date, only a limited number of computational models have been proposed that satisfy this.[18,19] Several models assess pulmonary function in hypertensive diseases using explicit representations of the major pulmonary arteries combined with lumped models of the distal vasculature.[20,21] This provides an accurate representation of macrovascular structure and function, but neglects the anatomical detail of the small pulmonary blood vessels where significant vascular remodeling occurs.[22] Qureshi et al.[23,24] explicitly represented the geometry of the first three generations of pulmonary arteries, but simplified the rest of the pulmonary vasculature as a structured bifurcating tree (a quasi-symmetric structure). CTEPH has been represented by increasing the stiffness of the large pulmonary arteries,[24] and more recently by hemodynamic models of occlusions typical of the disease.[23] PAH typically is modeled by stiffening of small pulmonary arteries.[24,25] Vascular asymmetry across relevant scales to CTEPH and PAH and the impact of vascular occlusion versus remodeling and physiologically relevant scales has not been considered. Asymmetry in structure across the whole vascular tree is required in a model to achieve this.[26] Clark and Tawhai[25] provide an imaging and morphometry-based model of the pulmonary vasculature that allows prediction of blood flow dynamics that incorporates anatomical structure from the heart to the pulmonary capillaries, as well as the considerable impact that gravity and local tissue elastic recoil pressure have on pulmonary vascular function. This allows a basis for a systematic investigation of the impact of microvascular remodeling and macrovascular occlusion in human lungs.

In this study, we present a computational model to simulate the impact of distal remodeling on the MPA impedance. The model provides an integrated assessment of vascular function including anatomic branching of blood vessels, the effect of gravity, and distensible and recruitable capillary beds. The model is used to investigate differences between PAH and CTEPH. In this work, we have implemented a staged description of vascular remodeling based on a detailed histological study.[22] We use the model to interpret how dynamic measurements of hemodynamics at the right heart reflect distal and proximal vasculopathy typical of PAH and CTEPH.

Methods

We employed an anatomical model of the entire pulmonary vasculature to understand its dynamic function in response to local and global pathology typical of PAH and CTEPH. This model builds upon previously published anatomical models of pulmonary vascular function.[18,25,26]

Model geometry

The anatomically structured model of the pulmonary circulation consists of macrovascular, acinar, and capillary-scale components, as presented in previous studies.[25] The *macrovascular* component was derived from volumetric high-resolution computed tomography (CT) images of the lungs of a 23-year-old Caucasian, never smoking male with a body mass index of 23.1 kg/m^2 from the Human Lung

Atlas database.[27] Images were acquired at close to functional residual capacity. The subject was selected from a cohort of normal subjects aged 20–30 from this database as the closest to the mean shape derived from a principal component analysis of the cohort.[28] The macrovascular model includes arterial structure from CT to one generation beyond the segmental arteries, supplemented by a volume filling branching algorithm to create an arterial and venous tree geometry to the acinar level with morphometrically consistent properties.[18,26] The resulting geometry is a three-dimensional distributed graph-like structure with blood vessel structures described by their start point, endpoint, and radius. The repeated *acinar* structure is a nine-generation acinar branching model,[29] with discrete arterioles and venules that are connected by multiple parallel capillary connections, forming a ladder-like model. This acinar model lies distal to each terminal artery (of which there are ~32,000) in the macrovascular model. The *capillary* connections are conceptualized as recruitable capillary sheets, following the rigorous mathematical description for capillary beds derived by Fung and Sobin.[30–32]

Simulating dynamics of the pulmonary blood flow

Blood flow in the macrovascular, acinar, and capillary blood vessels was simulated using wave transmission theory.[25,32,33] Each blood vessel in the model that is proximal to the capillary beds was represented by a discrete compliant tube, and the capillary bed was represented via sheet flow theory. Details of the methodology are provided as Supplementary Material. Briefly, blood flow in the *extra-capillary vascular network*, was simulated by superposing a forward traveling flow waveform, backward traveling waveform and a steady state flow in the system. Blood flow through the branching network of pulmonary blood vessels was simulated using an electrical circuit analogue model, as described in full by Clark and Tawhai.[25] In this model, each extra-capillary blood vessel has associated with it a characteristic admittance (Y_c) and a characteristic wave velocity (c_0, the characteristic velocity at which a pulse of blood travels along the length of a blood vessel). This characteristic admittance is a function of vessel radius (r_0), vascular wall compliance (α_0, itself a function of vessel elastance and wall thickness), blood density (ρ), blood viscosity (μ), and frequency (ω). This characteristic impedance is the impedance that the individual vessel contributes to the system. The effective admittance (Y_e) of a vessel is a function of the characteristic admittance of all downstream segments calculated using connectivity of elements in series and in parallel.[25] Y_e is updated in each vessel as a function of the admittance in downstream vessels via formulae defined at bifurcations which take as inputs the relative radii of vessels in the network and the length of each vessel segment.[33–35] This effective admittance is then used to calculate the relationship between pressure and flow in the whole system (admittance is the ratio of flow to pressure). This is achieved by applying a boundary condition at the left heart outlet (see Boundary and initial conditions section) and calculating effective admittance in each vessel from the left heart back toward the right heart (the MPA inlet). Flow and pressure in each individual vessel are then calculated based on prescription of a boundary condition at the right heart (see Boundary and initial conditions section).

The equations governing the dynamics of blood flow in the *pulmonary capillaries* were derived via the theoretical analysis of Fung,[32] allowing for a change in capillary diameter across the capillary sheet (accounting for compliance of a two-port network). This approach differs from the model described by Clark and Tawhai[25] who did not allow for a mismatch in arterial and venous blood pressures at the inlet and outlet of the capillary sheet, but is consistent with previous modeling of the pulmonary vasculature that used simplified representations of macrovascular structure.[34,35]

Boundary and initial conditions

Boundary conditions were specified at the MPA (the inlet to the model) and the pulmonary veins (the outlet to the model).

The incident flow waveform in the MPA was defined as a cosine Fourier series

$$q_0(t) = \sum_{n=1}^{N} A_n \cos(\omega_n t + \phi_n) \quad (1)$$

where ω_n is the nth harmonic frequency ($\omega_n = 2\pi nHR/60$, with HR as heart rate), A_n is an amplitude, and ϕ_n is a phase offset. These parameters are defined in Table 1 for the first eight terms. The function $q_0(t)$ at the MPA inlet is the equivalent of the forward traveling flow waveform provided by the heart for the system; this waveform was assumed to be fixed across simulations. Interpreted physically, a fixed flow waveform assumes that the heart can continue to generate the same cardiac output, independent of pulmonary vascular disease. This forward waveform was generated by simulating flow in the normal lung under conditions described by Clark and Tawhai[25] and then holding this waveform fixed across all further simulations. The assumed waveform magnitude spectrum is in good agreement with normal recordings of flow waveforms (when combined with backward waveforms produced within the

Table 1. Parameters defining forward flow waveforms at the main pulmonary artery (inlet).

n	1	2	3	4	5	6	7	8
ω_n	7.54	15.08	22.62	30.16	37.70	45.24	52.78	60.32
A_n	10.42	5.44	3.08	0.55	0.57	0.85	0.44	0.30
ϕ_n	−1.95	−2.56	2.94	1.82	−1.33	−2.42	2.98	−1.12

n being the harmonic frequency number, ω_n is harmonic frequency, A_n is defined in l/min, and ϕ_n is in radians.

lung) and simulations of forward flow waveforms derived by other studies.[19] An analysis of the impact of decreased cardiac output on results is provided as Supplementary Material.

Zero wave reflection was imposed at the left atrium as a boundary condition (exiting the veins and entering the left atrium).[25] This has been tested against a load impedance condition at the left atrium with negligible impact on model predictions.[25]

Vascular compliance

The pulmonary blood vessels have elastic walls, enabling them to respond to changes in blood pressure over a cardiac cycle. The compliance of the pulmonary blood vessels is modified during the progression of vascular remodeling, due to early thickening of the arterial walls and later fibrosis.[22] For extra-acinar vessels (arteries and veins), the relationship between radius (r) and transmural pressure (P_{tm}) is defined as

$$r = r_0\left(1 + \frac{3r_0}{4Eh}\right)P_{tm} = r_0(1 + \alpha_0 P_{tm}) \tag{2}$$

where E is the Young's modulus, r_0 is the unstrained radius, α_0 is the vessel compliance, and h is the thickness of the vessel wall, respectively.

At the capillary-scale, the sheet height, H, is a function of the transmural pressure, defined by

$$H = H_0 + \alpha_c P_{tm} \tag{3}$$

where α_c is a compliance constant, and H_0 is the unstrained sheet height.[30] For blood vessels with diameter less than 200 μm, P_{tm} is defined as the difference between blood pressure and the air pressure in the surrounding alveolar tissue. In larger vessels, it is defined as the difference between blood and local tissue elastic recoil pressure.[31,36,37]

Model implementation and baseline parameterization

The model was implemented using a custom-written Fortran library, accessible via a python interface and installable as a python library (www.github.com/LungNoodle/lungsim). The differential equations associated with Fung's mathematical description of the capillary beds[32] were solved using a finite difference method. The parameters used in this model are shown in Table 2,[18,31,34,41–43] following the steady-state description of the lung given by Clark et al.[18]

Perturbations to the model to reflect vascular pathology

We considered two perturbations to the model to reflect the vascular pathology typical of PAH and CTEPH: vascular occlusion and vascular remodeling. We considered these perturbations separately and together. Selected scenarios are illustrated in Fig. 1. PAH was simulated by remodeling alone, divided into 10 steps from RM1 (normal) to RM10 (most severe). CTEPH was simulated by a combination of occlusion and remodeling (RM1-10) in the non-occluded regions.

Vascular occlusion was simulated using two scenarios: Case 1: left lower lobe (LLL) occlusion to reflect a major proximal occlusion of the pulmonary vasculature, and second, random occlusion of arteries one generation distal to the segmental level which reflects a more distal occlusion. Case 2: we occlude arteries until the total number of capillary beds that are occluded is as close as possible to the case where the LLL is occluded. Occlusion is simulated by reducing the diameter of an individual artery until simulated blood flow through that artery is negligible.[38,44–46]

Vascular remodeling is simulated via a staged description of vascular remodeling, as first described by Postles et al.,[39]

Table 2. Baseline model parameters, following Clark et al.,[18] which describe the normal structure and function of the pulmonary vasculature.

Parameter	Description	Value	Reference
R_0 (MPA)	Main pulmonary artery unstrained radius (mm)	11.2	
R_d (artery)	Strahler diameter ratio (arteries, no units)	1.52	18
R_0 (MPV)	Main pulmonary vein unstrained radius (mm)	14.53	
R_d (vein)	Strahler diameter ratio (veins, no units)	1.56	18
α	Vessel baseline compliance (Pa^{-1})	1.49×10^{-4}	41
μ	Blood viscosity (Pa·s)	3.36×10^{-3}	43
ρ	Blood density ($kg{\cdot}mm^{-3}$)	1.05×10^{-6}	43
α_c	Capillary sheet compliance ($m{\cdot}Pa^{-1}$)	1.3×10^{-9}	42
F	Friction factor constant (no units)	1.8	31
K	Friction factor constant (no units)	12.0	31
H_0	Unstrained capillary height (m)	3.5×10^{-6}	42
L_c	Average length of a capillary unit (m)	1186×10^{-6}	34
μ_c	Apparent blood viscosity in capillaries (Pa·s)	1.92×10^{-3}	42

MPA: mean pulmonary artery; MPV: mean pulmonary vein.

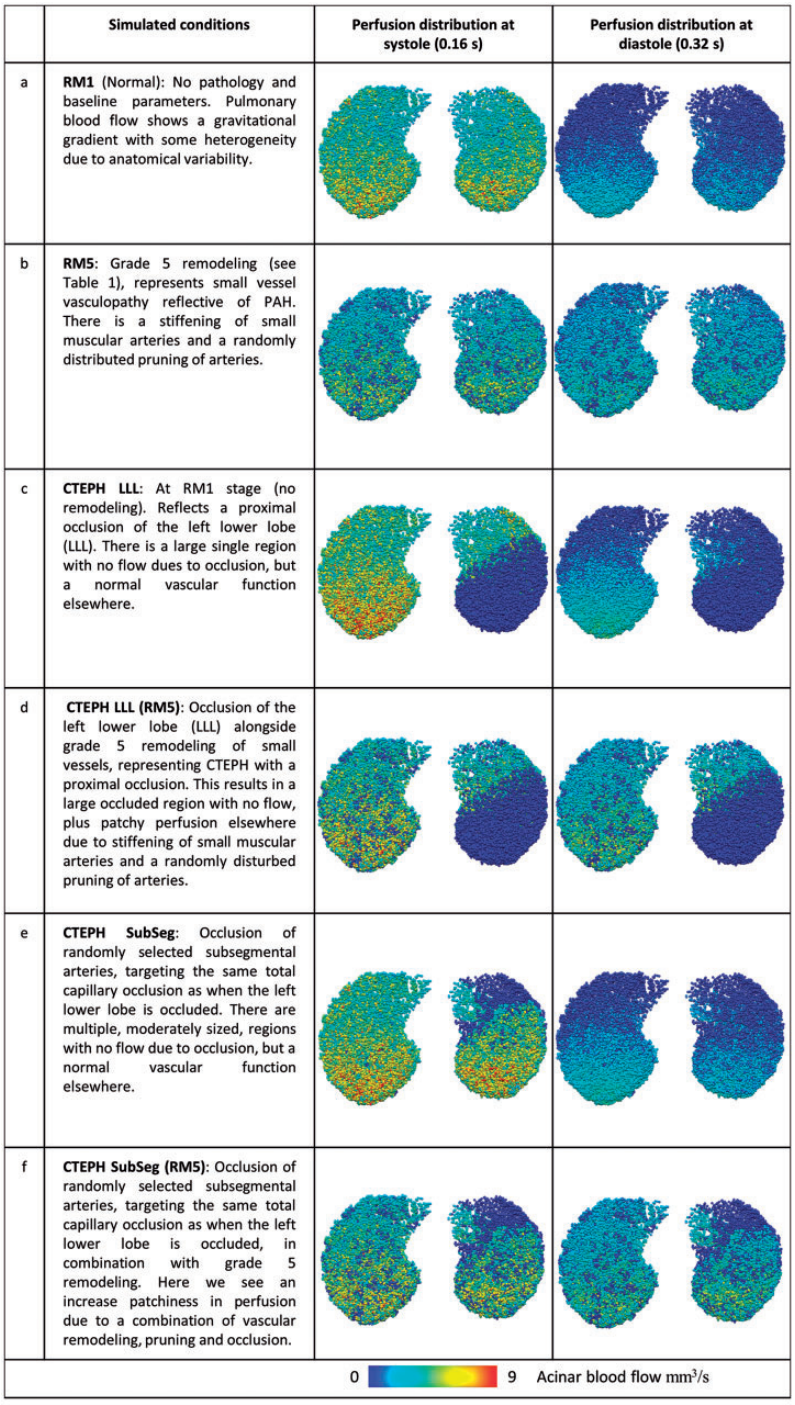

Fig. 1. Illustrations of key simulated scenarios and predicted blood flow distribution at the acinar level in two time steps of a heart cycle (0.16 s, representing systole and 0.32 s, representing diastole). Each simulated scenario aims to capture similar levels of pathological changes in the pulmonary vasculature but with different underlying distribution of disease. Row (a) shows the case of no pathology (RM1), (b) shows small vessel vasculopathy on grade 5 (see Table 1), (c) represents proximal left lower lobe occlusion with no vessel pathology (RM1 with occlusions), (d) shows with proximal left lower lobe occlusion along with RM5 remodeling, (e) shows occlusions in subsegmental arteries occluding the same number of capillaries as panel (c) with no pathology, and (f) shows subsegmental occlusions same as panel (e) with RM5 remodeling.

assuming that the remodeling process in CTEPH and PAH happen via the same stages.[40,47] The structural evolution of small pulmonary blood vessels during remodeling was assessed by Heath and Edwards in a detailed histological study in idiopathic PAH.[22] Remodeling was classified into six grades with increasing severity, but we exclude Grade 6, which involves necrotizing arteritis and is rare.[30] We split the five grades of remodeling into 10 steps (two per grade).

Remodeling is characterized by reductions in compliance due to (1) hypertrophy and hyperplasia (α_h), and (2) fibrosis (α_f) along with application of a narrowing factor due to proliferation of the intima (n_f) and a pruning factor related to occlusion of the vessels (p_f), summarized in Table 3. These factors modify the radius-compliance relationship defined in equation (4) to

$$r = n_f r_0 (1 + \alpha_h \alpha_f \alpha_0 P_{tm}) \quad (4)$$

A detailed rationale for the parameterization given in Table 3 is provided as Supplementary Material.

Model analysis and relation to information typically derived from right heart catheterization

The model predicts blood flow and pressure variation at each level of the pulmonary vascular tree. This allows assessment of the distribution of pulmonary blood flow and calculation of key metrics that have been previously derived from right heart catheterization (RHC) data. Here we use our model to predict:

1. *mPAP and pulmonary vascular resistance*
2. *Spectra representing the impedance magnitude and phase* in the MPA. Impedance is the ratio of flow to pressure, and can be decomposed into magnitude and phase components, which in turn depend on frequency. Typical impedance spectra are classified by a high zero frequency impedance, followed by a minimum in low frequency (1–3.5 Hz),[48] and then oscillation around an asymptote.[49–52]
3. *A normalized pulse pressure* which represents the difference in the systolic (peak) and the diastolic (minimum) pressure, normalized by mPAP.
4. *Wave speed, forward compressive wave (FCW) intensity, and backward wave (BW) intensity* which can be derived from a wave intensity analysis.[6,7,24] Each of these metrics has been proposed as a means to distinguish between disease presentations based on observed differences between PAH and CTEPH cohorts.[6]

Results

Fig. 1 shows a selection of simulated conditions and physiological interpretation for each of these conditions. This illustrates how vascular remodeling alone impacts the predicted distribution of perfusion in the lungs at near-systole and near-diastole time-points. As remodeling is progressively implemented, the predicted distribution of perfusion transitions from a gravitationally dependent distribution, with local heterogeneity due to asymmetry in vascular structure, to a 'patchier' distribution of perfusion with reduced gravitational dependency. Where proximal occlusion is added to the model (CTEPH), we see increased disruption to the perfusion distribution, in localized regions.

Fig. 2 shows the simulation results, with blood flow per acinus (perfusion) averaged in 10 mm bins along gravitational height of the lung. When remodeling (alone) is implemented in the model, there is an increase in the isogravitational heterogeneity of perfusion (quantified by standard deviation) and a decrease in the temporal variation in blood flow. That is, systolic and diastolic flow magnitudes are closer together. The same trends are apparent in CTEPH simulations which include occlusion, but the magnitude of heterogeneity in perfusion is greater. When the left lower lobe alone is occluded this heterogeneity presents in a localized region at the base of the lung, but when subsegmental arteries are occluded this heterogeneity is present throughout the whole lung.

Fig. 3 shows static (mPAP) and dynamic pressure profiles predicted by the model as a function of the ten prescribed remodeling stages (RM1-10). Fig. 3a shows a moderate increase in mPAP in the early stages of disease (prior to RM5), but as vascular pruning and stiffening due to fibrosis are introduced, predicted mPAP increases beyond the level that normally results in diagnosis of PH

Table 3. The parameters defining the simulated 10 steps of remodeling, following Postles et al.[39]

Grade (remodeling step, RM)	α_h	n_f	p_f	α_f	Notes
1 (RM1)	1	1.0	0.0	1	Normal pulmonary vasculature (no remodeling)
1 (RM2)	5/6	1.0	0.0	1	Small changes in compliance due to hypertrophy
2 (RM3)	2/3	0.925	0.0625	1	Vessel narrowing and pruning begins to play a role
2 (RM4)	1/2	0.850	0.1250	1	
3 (RM5)	1/3	0.775*	0.1875*	1	Vascular pathology begins to influence larger vessels (<500 μm)
3 (RM6)	1/6	0.700*	0.2500*	5/6	Fibrosis begins to influence vascular compliance
4 (RM7)	1/6	0.625*	0.3126*	2/3	
4 (RM8)	1/6	0.550*	0.3750*	1/2	
5 (RM9)	1/6	0.550*	0.4375*	1/3	Severe fibrosis with vessels <1000 μm impacted
5 (RM10)	1/6	0.550*	0.5000*	1/6	

A reduction in compliance due to hypertrophy and hyperplasia, α_h is applied to vessels in the diameter range 100–1000 μm. A narrowing factor due to proliferation of the intima n_f is applied to vessels in the diameter range 30–300 μm, or 30–500 μm for values with an asterisk. A pruning factor representing complete occlusion of the vessels, p_f, is applied to vessels of diameter <300 μm, or <500 μm for values with an asterisk. Finally, a reduction in compliance due to fibrosis, α_f, is applied to vessels in the diameter range 30–500 μm.

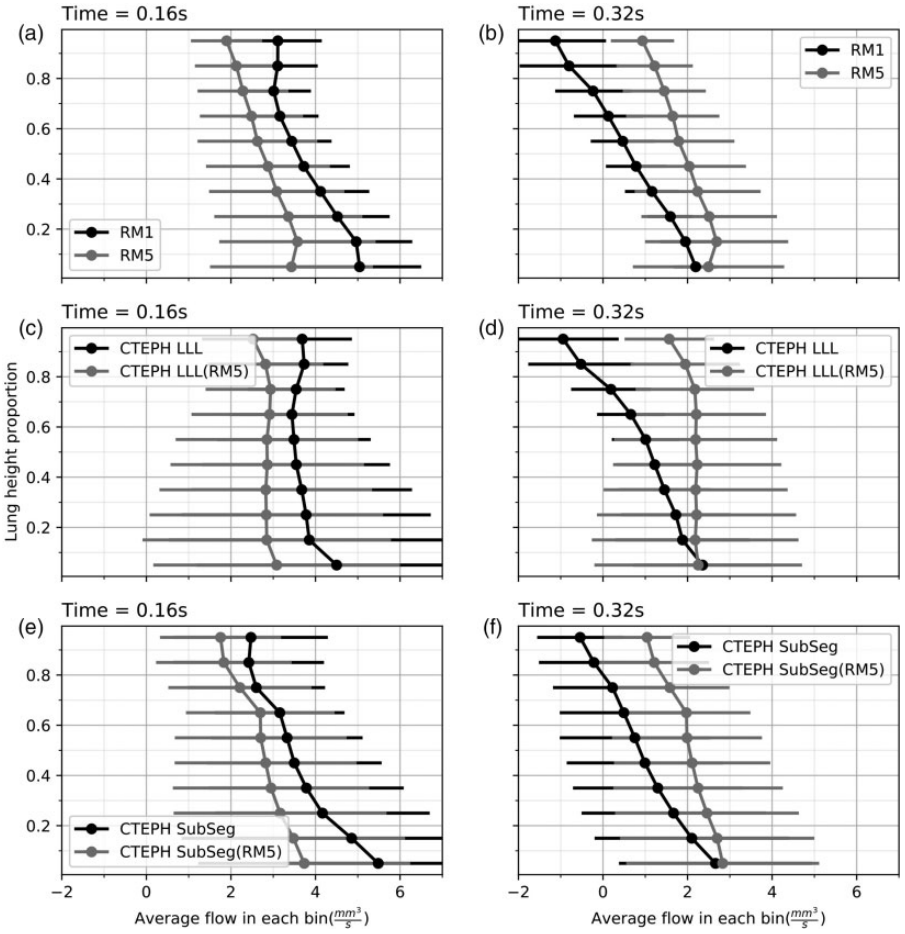

Fig. 2. Simulated acinar perfusion distribution averaged in 10 mm bins versus normalized height of the lung, in the direction of gravity. (Top row) Average flow distribution for healthy and PAH stage 5 (RM5, as defined in Table 3) at two time-points of the heart cycle, representing near-systole (0.16 s) and near-diastole (0.32 s). (Middle row) Average flow distribution for proximal left lower lobe occlusions (CTEPH LLL) at RM1 and RM5. (Lower row) Average flow distribution for distal sub-segmental occlusions (CTEPH SubSeg) at RM1 and RM5.

(indicated by a horizontal dashed line). In the case of CTEPH simulations, occlusion of the LLL or the subsegmental arteries increases overall mPAP but the trends in mPAP with level of remodeling remain similar to the case of remodeling alone. The dynamic pulmonary artery pressure profiles increase in amplitude progressively over the simulated remodeling stages (Fig. 3b), again with the largest increases occurring after RM5 (where fibrosis and significant vascular pruning is introduced). CTEPH simulations show similar trends in pressure waveforms (not shown), but visually distinguishing between these waveforms would not be possible in investigation of clinical pressure traces.

Fig. 4 shows the nature of impedance magnitude as predicted by the model. All spectra exhibit a high impedance at zero frequency values (representing the pulmonary vascular resistance, the non-transient component of impedance). As expected, the magnitude of this zero frequency impedance increases with increasing severity of vascular remodeling (Fig. 4a). For the lower remodeling stages (RM1 to RM5), impedance spectra show a minimum around 1–3.5 Hz, and a second peak between 4 and 8 Hz. However, alongside an increase in magnitude we predict a shift to the right of the impedance spectra with increasing remodeling stage, which is typical of those seen in PAH.[53] Although inclusion of occlusion, as in CTEPH, modifies impedance spectra by elevating peaks there is no clear distinction between PAH and CTEPH in terms of the nature of these impedance spectra.

Recent studies have suggested that a more complex interpretation of pulmonary artery pressure and flow waveforms may better distinguish between etiologies of PH.[2,3,7] This includes calculation of normalized pulse pressure and wave intensity analysis. The wave speed, the intensity of the forward compressive wave (FCW), and the backward wave (BW) are key metrics from this analysis that could be used to distinguish between disease presentations.[6] Fig. 5 takes these metrics, plus the location of the first minimum in the impedance spectra and the height of the first peak and plots against mPAP to determine whether any of these metrics are able to distinguish between predicted metrics in the

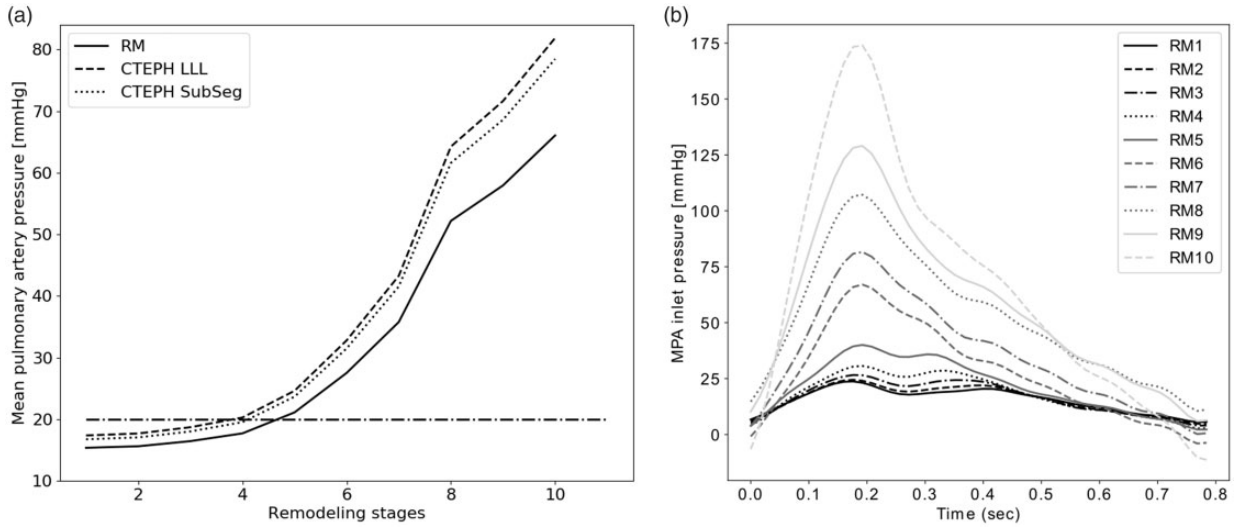

Fig. 3. (a) Model predicted mPAP as a function of remodeling stages, for simulations of PAH and vascular remodeling plus occlusion (CTEPH). Remodeling stage 1 (RM1, Table 3) represents a healthy vasculature and stage 10 (RM10, Table 3) the most severe case simulated. (b) Main pulmonary artery net pressure for simulations of PAH, at each level of remodeling (RM), from RM1 being the healthy and RM10 being the most severe case, CTEPH simulations are not shown but are comparable.

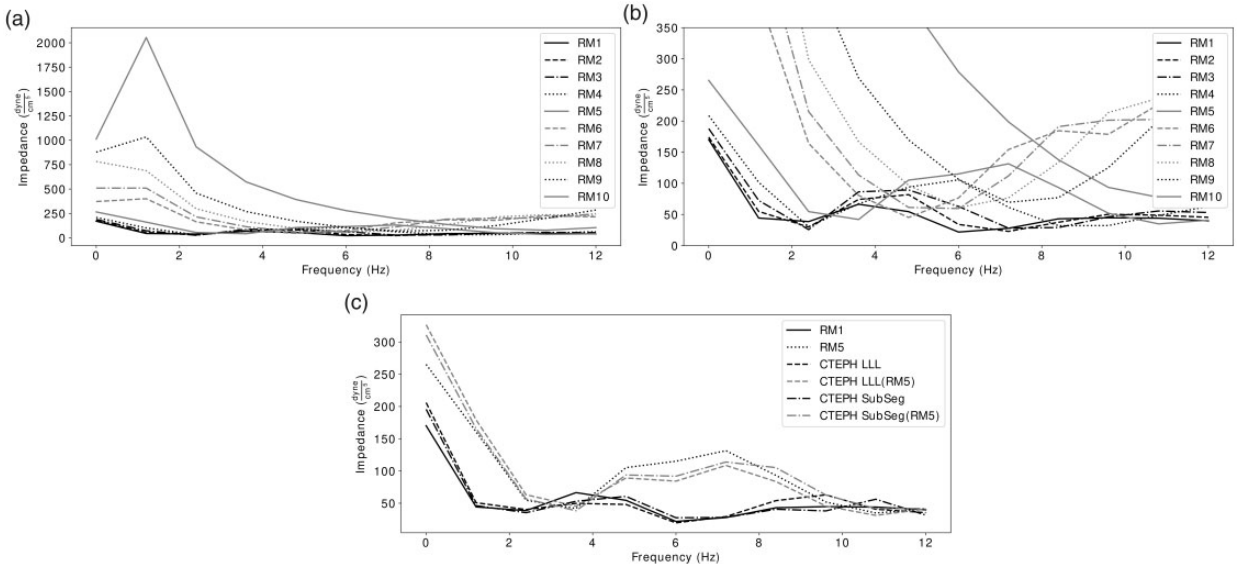

Fig. 4. A comparison of main pulmonary artery impedance versus harmonic frequency (Hz) for PAH and CTEPH simulations. (a) Impedance spectra with changes in remodeling stages from healthy to the most severe remodeling stage (RM10). (b) Impedance spectra of the same remodeling stages as panel (a) to magnify the changes in lower values of impedance and show a comparison between different PAH stages in the main pulmonary artery impedance. (c) A comparison of impedance spectra between healthy, PAH and CTEPH. *RM5, PAH with remodeling stage 5; *CTEPH LLL, Left lower lobe occluded CTEPH (proximal occlusion); *CTEPH SubSeg, Sub-segmental occlusion CTEPH (distal occlusions).

MPA in simulations of PAH and CTEPH. The normalized pulse pressure increases in early stages of remodeling where remodeling is limited to hypertrophy and proliferation of the intima, but as remodeling progresses the whole system effectively becomes stiffer and the normalized pulse pressure begins to decrease (Fig. 5a). For the same pulmonary artery pressure, we predict a reduced normalized pulse pressure in CTEPH due to proximal occlusions. Metrics derived from wave intensity analysis (Fig. 5b-d) show that in general our model predicts lower FCW intensity and BW intensity in CTEPH than in PAH. However, because the relationship between these metrics and mPAP is non-linear it may be difficult to use these metrics to distinguish between individual patients. Finally, we see a shift in the location of the first impedance spectrum minima to the right (Fig. 5e) in both PAH and CTEPH, and an increase in the magnitude in the secondary peak with increasing mPAP. In this metric we see a consistent trend, that for a given mPAP the secondary

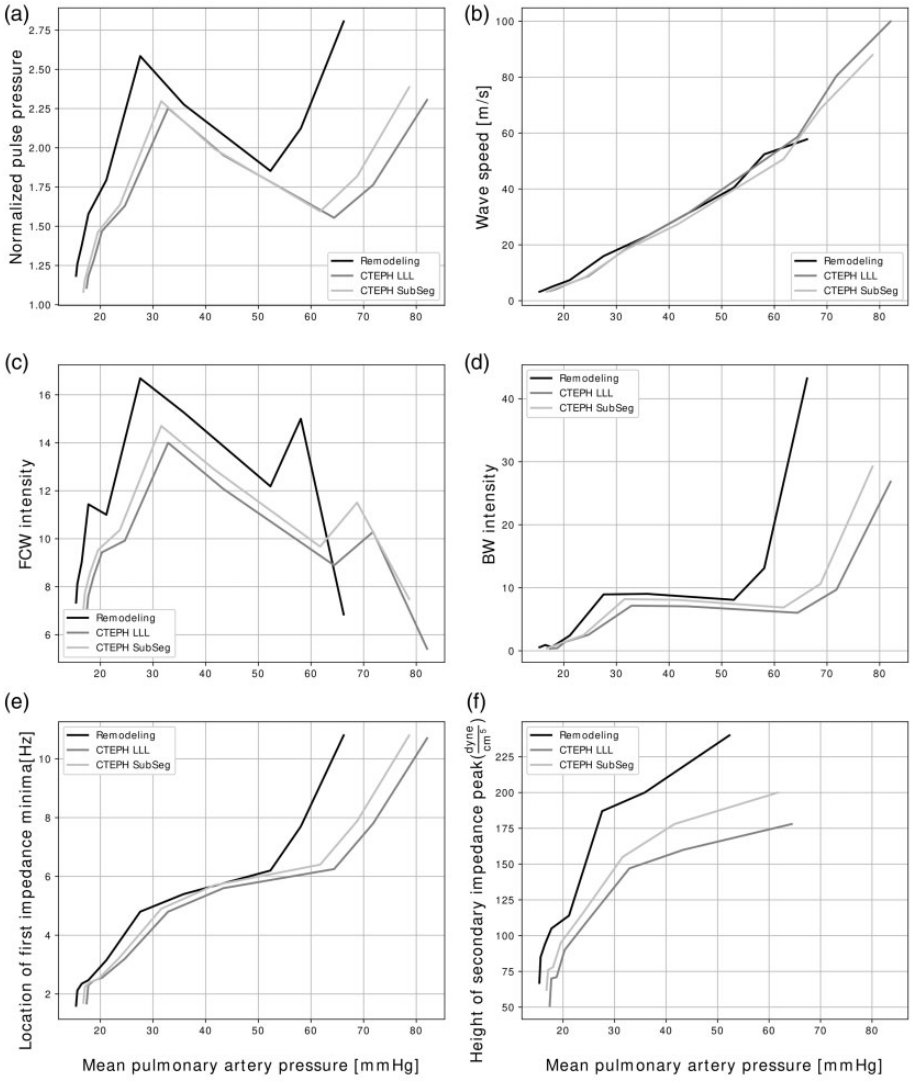

Fig. 5. (a) Normalized pulse pressure at inlet of main pulmonary artery (MPA) versus mean pulmonary artery pressure (mPAP). Increase in mPAP is due to increase of remodeling for PAH, proximal CTEPH (CTEPH LLL) and distal CTEPH (CTEPH SubSeg). (b) Wave speed at MPA with increase of remodeling in PAH, CTEPH LLL and CTEPH SubSeg. (c) Forward compression wave intensity at MPA against mPAP for PAH, CTEPH LLL and CTEPH SubSeg. (d) Backward compression wave intensity at MPA against mPAP for PAH, CTEPH LLL and CTEPH SubSeg. (e) Shows which frequency the impedance is having its first minimum against mPAP for PAH, CTEPH LLL and CTEPH SubSeg. (f) The secondary impedance peak value for PAH, CTEPH LLL and CTEPH SubSeg against mPAP. This graph does not have the values for the second peak in higher mPAP since the impedance in those stages does not experience a second peak within the limits of harmonic frequency considered (see Fig. 4b).

peak will be lower in CTEPH than in PAH, and this effect will be amplified the more proximal the occlusion (Fig. 5f). We note (Supplementary Material) that decreases in cardiac output result in increases in normalized pulse pressure and FCW, with minimal impact on other parameters. This suggests that these two indices likely increase with disease severity beyond the stage that the heart maintains its normal cardiac output.

Discussion

In this study we presented a computational model of the pulmonary vasculature that aims to capture changes to the vasculature in PH, with a particular focus PAH and CTEPH. The anatomically based computational model employed in this work has successfully linked large scale measurements of pulmonary vascular function, and changes in the pulmonary microvasculature as a consequence of vascular remodeling in disease. The model suggests that dynamic measurements of blood pressure and flow at the right heart potentially distinguish between distal and proximal vasculopathy typical of PAH and CTEPH. We assessed several metrics of vascular function that can be calculated from RHC data and conclude that nonlinearity in response to changes in vascular structure may impede analysis and interpretation of these metrics between cohorts.

Previous computational studies analyzing functional differences between PAH and CTEPH have used a quasi-symmetric structure to represent the pulmonary arteries and veins, and represented CTEPH and PAH as an increased stiffness in the pulmonary arteries (CTEPH by stiffening large arteries, and PAH by stiffening small arteries).[24,25,54] Our anatomical description of the pulmonary vascular structure allows us to explicitly simulate how the distribution of vascular remodeling and macrovascular occlusion in the lungs impacts vascular function, due to explicit representation of vascular branching to the acinar level. Rather than assuming vascular remodeling to be simply a stiffening of the pulmonary arteries,[19,25,33,55] we implemented a staged vascular remodeling phenotype based on histological imaging.[22] This aims to capture the contributing factors to the pathogenesis of PAH which includes both a stiffening of the vasculature due to changes in vessel wall structure and fibrosis, and a microvascular 'pruning' or loss of patency of the small blood vessels.[56,57] Our implementation of CTEPH in this model as a combination of occlusion and small vessel remodeling reflects current understanding of its pathophysiology, which describes the disease as often arising from prior thrombi in large or medium sized vessel causing high vascular resistance accompanied by small vessel disease.[11,40,56,58,59] With this integrated model of the pulmonary vascular system, it is possible to analyze the impacts of disease processes at different spatial scales (proximal occlusion versus distal remodeling) and how this may impact clinically measurable quantities. This approach opens the door to 'personalized' modeling of patients with PAH and CTEPH, as has been demonstrated in pulmonary embolism cases [38] which can assess how heterogeneity in disease presentation impacts function. However, the focus here is to determine how typical disease presentation impacts on RHC metrics and so a single anatomically based vascular geometry is assessed with different disease presentations imposed within it.

Some forms of PH present with lower mPAP than meet the diagnosis threshold.[1,60] For example, some patients with pulmonary vascular dysfunction present with exercise limitation, at lower resting mPAPs.[1,60] This is consistent with our model predictions that show a non-linear trend for elevation in mPAP with vascular remodeling, indicating that significant small vessel vasculopathy can be present prior to reaching an abnormal mPAP. Trends in mPAP are also consistent with previous model studies showing the impact of vascular occlusion in acute pulmonary embolism, with substantial increases in mPAP being a factor only when significant occlusion is present.[38] Predicted impedance spectra are also consistent in shape and magnitude to those typically derived in the pulmonary circulation in health and pulmonary vascular disease.[53] In normal function, the first minimum in the impedance spectrum is described as being at 2–3 Hz, and shifts to the right in PH.[53] This shift to the right is described as being indicative of a poor right ventricular coupling with the pulmonary circulation.[53] The trends observed in our impedance spectra in response to imposed pulmonary vascular changes are therefore as expected, with a shift to right in phase and impedance spectra with increase of magnitude of oscillations in more severe remodeling cases (higher distal vessel compliance and vascular pruning). There are simulated cases where the magnitude of increase in mPAP and the amplitude in oscillation of pulmonary artery pressure become non-physiological. This occurs approximately at our remodeling stage 8 where there is significant vascular pruning and compliance reduction, and mPAP elevates beyond the upper range of 46.1 ± 11.4 mmHg that has been reported in the literature.[61] This overestimation of mPAP in the most extreme cases simulated is likely a result of vascular remodeling being imposed equally throughout the lung model (so there is no regional variability in disease presentation), as well as an assumption that cardiac output is not impacted by late-stage disease. In reality, the heart compensates for the increased downstream resistance by remodeling, leading to increased cardiac wall thickness and hypertrophy.[21,48,62] In chronic PH a decrease in cardiac output due to these factors is expected.[62–64] However, it is beyond the scope of this study to attempt to model cardiac remodeling in response to PH, and as such this model provides an upper limit for the pressure response to vascular pathology within the lungs.

An important benefit of the proposed model is that it can simulate the response of the pulmonary vasculature to different distributions of disease. In the scenarios considered (illustrated in Figs. 1 and 2) we simulate perturbations to the pulmonary vasculature with different regional distributions that result in similar elevations in pulmonary vascular resistance. The first, small vessel vasculopathy (simulated throughout the lung) is reflective of PAH, and the other scenarios simulated aim to reflect CTEPH with vascular occlusion superimposed on small vessel vasculopathy. In the CTEPH scenarios we consider a large proximal occlusion and more distributed subsegmental occlusions. The differences in mPAP predicted in these scenarios are small; however, the impact of these imposed pathologies on both the spatial and temporal distributions of perfusion within the lung show major differences. Regions with lower flows (anterior in supine) demonstrated the most temporal changes in both health and disease which is consistent with the literature.[65,66] When spatial heterogeneity is introduced to the model via vascular occlusion, our model predicts an increase in temporal variability in perfusion alongside this spatial heterogeneity (see Fig. 2). While a vertical gradient of perfusion is evident in normal human lung, this is obscured in spatially uniform disease (see Fig. 2) which is consistent with experimental measurements from the literature.[67,68] Patchiness in flow distribution is a frequently reported outcome of CTEPH.[69]

A mosaic like pattern on chest CT scan is not in itself specific to a subtype of PH, but the correlation between a mosaic pattern and sub-segmental perfusion defects is likely to connect small vessel disease (in our case PAH or CTEPH) to more proximal pulmonary artery dilation.[69] Mosaic pattern attenuation has been proposed as an easy method to evaluate blood distribution of CTEPH patients,[70] although it can arise from vascular remodeling in the absence of vascular occlusion.[25]

This study has presented the impact of disease distribution on dynamic markers of pulmonary vascular function, that may contribute to diagnosis and differentiation of PH. As a part of wave intensity analysis, calculation of a wave speed (or pulse wave velocity) is typical.[7] Wave speed can be reliably calculated from RHC measurements, and is significantly higher in PH patients than in controls.[7] Wave speed has been shown to be elevated in both CTEPH and PAH patients, but no significant differences have been found between the two groups.[6] Our model suggests that wave speed is strongly correlated with mPAP and that differences in wave speed between CTEPH and PAH differ only marginally, despite this metric being strongly related to the presence or absence of PH (see Fig. 5b). Similar to clinically measured pulsatility index (pulmonary artery pulse pressure normalized by right atrial pressure), normalized pulse pressure is defined to provide a measure of downstream dynamic resistance. Pulsatility indices have been shown to be a marker of right ventricular dysfunction[71] and are elevated in CTEPH compared with PAH patients (although some studies do not control for mPAP).[72,73] While FCW intensity has been reported to be higher in both PAH and CTEPH than in normal controls, there has been no reported significant difference between CTEPH and PAH.[6] Our model predicts that for a given mPAP both normalized pulse pressure and FCW are expected to be higher in CTEPH than in PAH, and may distinguish between cases if a depression in cardiac output is observed. On the other hand, BW intensity shows consistent trends across the scenarios simulated, showing a trend for an increase as mPAP increases, and a consistent reduction in simulated CTEPH scenarios compared with PAH simulations. This is consistent with observed reductions in BW intensity in CTEPH but not in PAH derived from clinical data (although these differences were not statistically significant).[6] Our model suggests that the impact of the proximal occlusions typical of CTEPH can be seen in impedance spectra characteristics, and that for a given measured mPAP one would expect the first minimum of the impedance spectra to be further to the left than in PAH, and the secondary maximum to be lower in height. The fact that model predictions consistently show this trend, for the range of small vessel vasculopathies simulated, suggest that these characteristics of the impedance spectra, along with BW intensity derived from wave intensity analysis are potentially likely indicators of differences between a distal presentation of disease more typical of PAH and a proximal contributor as observed in CTEPH. The choice of such a marker clinically is a factor of both their ease of calculation and their ability to distinguish between populations.[74] Computational modeling provides an avenue to improve interpretation of these data in cohorts presenting with different PH etiologies.

Model limitations

The model assumes Newtonian behavior of blood in the extra-acinar blood vessels, and non-Newtonian behavior in the micro-vasculature that is approximated by an assumption of an effective blood viscosity (derived from empirical data) at this scale.[18,25] Assumptions were made while developing the wave transmission theory in the tree that the equations representing blood flow can be linearized and that there is no 'multiple wave reflection' (the first reflection is dominant). This is consistent with previous studies that the primary reflection is dominant, particularly in proximal arteries.[3,75]

In analysis of the impact of occlusion on the lung, a target proportion of the lung was occluded, rather than conducting a physiological assessment of the regions of the lung most likely to be occluded (e.g. due to the distribution of blood flow in the lung). A previous study,[54] considering occlusion alone in the left and right lower lobes, indicated a slightly higher impact of right lower lobe occlusion than left, but trends in functional metrics with remodeling are similar. In this analysis we imposed complete occlusion to simplify comparisons between clustered and more diffuse occlusion; however, simulation of partial occlusion is possible using methods employed by ourselves[38] and other groups.[23] Our previous analysis in acute pulmonary embolism suggests that partial occlusion of an artery has a non-linear impact on hemodynamics with roughly 50% or more occlusion being hemodynamically significant at the MPA. However, partial occlusion that allows flow to reach the small remodeling arteries may impact their remodeling and this would be an interesting focus for future studies.

The model also neglects heterogeneity in arterial changes in PAH, which may arise from different disease phenotypes.[76] The staged structural analysis of Heath and Edwards provides a detailed structural analysis that can be directly related to parameters defining vascular size and compliance.[22] More recent studies[76] add detail on fraction intima and media thickness (which influence h in equation 2) subphenotypes of PAH and healthy lungs. Overall, the changes in fractional wall thicknesses are comparable with our change in compliance implemented. However, it is clear that there may be vascular changes that do not exactly follow the stages defined by Heath and Edwards, for example plexiform lesions may form without significant remodeling. Similar studies that track

vascular changes by stage of disease may be useful to improve parameterization of the model in the future.

A further limitation of the model is the absence of a heart model at the inlet/outlet of the system that can adapt to changes in the pulmonary vascular system. Hence, the model is limited to assumptions regarding the cardiac response to elevated pulmonary blood pressure, as are all models assessing disease distribution to date.[16,18,19,23–25,36,38,77] Here, cardiac output is held constant throughout all the case studies, which could lead to an over-estimation of both mPAP and pulse pressures in some cases. In addition, clinically measured pulsatility indices, which normalize by right atrial pressure, cannot be directly calculated by our model which is limited to assessing normalized pulse pressure as a proxy measure. In reality, the late-stage disease cardiac output is likely to decrease.[62–64] However, the non-linearities in predicted indices typically appear at pulmonary artery pressures below that which would indicate late stage disease, so this assumption primarily impacts the most extreme cases simulated. In the future, coupling our pulmonary model to a simple cardiac system model,[78,79] could improve the accuracy of model predictions when significant remodeling is present. Some simulations indicating how reductions in cardiac output influence key output metrics from our model are provided as Supplementary Material, including a preliminary illustration of how patient specific pathology and measured cardiac output can be combined to predict patient status. Inclusion of cardiac function into models of the pulmonary circulation in hypertensive disease should be an important focus for future modeling to avoid assumptions regarding this adaption.

In summary, our model predicts that there are potentially quantifiable differences in metrics reflecting the dynamic relationship between blood pressure and flow in the MPA between CTEPH and PAH, but that these differences should be interpreted with care, particularly when metrics representing this dynamic response change non-linearly with disease progression (for example when fibrotic changes begin to occur in the vasculature). Future studies that employ similar computational modeling techniques in a subject-specific context (as has been demonstrated in acute pulmonary embolism[38]) may provide a means to quantify heterogeneity in response to these conditions and to improve interpretation of proposed metrics of pulmonary vascular health.

Conflict of interest

Eric Hoffman is a founder and shareholder of VIDA Diagnostics, a company commercializing lung image analysis software developed, in part, at the University of Iowa. The other author(s) declare that there is no conflict of interest.

Ethical approval and consent

Patient-based model presented in Supplementary Material: Patients underwent right heart catheterization and computed tomography imaging at Auckland City hospital. The Northern X Regional Ethics Committee (NTX/09/08/074) and the Auckland District Health Board Research Review Committee approved use of the clinical data, and all subjects provided informed consent for participation in our study.

Funding

The author(s) disclosed receipt of the following financial support for the research, authorship, and/or publication of this article: This research was funded by the New Zealand Ministry of Business, Innovation and Employment's Catalyst Strategic fund, the Medical Technologies Centre of Research Excellence (Flagship 1, MHT principal investigator) and ARC was supported by a Royal Society Te Apārangi Rutherford Discovery Fellowship (14-UOA-019). Imaging was supported, in part, by NIH R01HL112986.

Author contributions

BSE: Conceived study, derived computational model, data analysis, wrote first draft of paper, edited and reviewed paper draft. MHT: Conceived study, contributed to computational model, contributed to computational tool development, edited and reviewed paper draft. HK: Conceived study, contributed to computational model, contributed to computational tool development, data analysis, wrote first draft of paper, edited and reviewed paper draft. KSB: Contributed to computational model, contributed to computational tool development, edited and reviewed paper draft. EAH: Collected Human Lung Atlas data, contributed image analysis tools, interpreted data in a physiological context, edited and reviewed paper draft. MLW: Conceived study, collected clinical data, interpreted data in a clinical context, edited and reviewed paper draft. DM: Conceived study, collected clinical data, radiologically assessed CT data acquired at Auckland City Hospital, interpreted data in a clinical context, edited and reviewed paper draft. ARC: Conceived study, derived computational model, data analysis, contributed to computational tool development, wrote first draft of paper, edited and reviewed paper draft.

Acknowledgements

We thank the anonymous referees for their useful insights and suggestions. We also thank contributors to the Human Lung Atlas Database as well as colleagues at Auckland City Hospital who have contributed their time to acquiring imaging and functional data.

ORCID iDs

Behdad Shaarbaf Ebrahimi https://orcid.org/0000-0001-6254-6226

Alys R. Clark https://orcid.org/0000-0001-5908-2862

Supplemental Material

Supplemental material for this article is available online.

References

1. Hoeper MM and Humbert M. The new haemodynamic definition of pulmonary hypertension: evidence prevails, finally! *Eur Resp J* 2019; 53: 1900038.
2. Hunter KS, Lee P-F, Lanning CJ, et al. Pulmonary vascular input impedance is a combined measure of pulmonary vascular resistance and stiffness and predicts clinical outcomes better than pulmonary vascular resistance alone in pediatric patients with pulmonary hypertension. *Am Heart J* 2008; 155: 166–174.
3. Huez S, Brimioulle S, Naeije R, et al. Feasibility of routine pulmonary arterial impedance measurements in pulmonary hypertension. *Chest* 2004; 125: 2121–2128.
4. Chemla D, Castelain V, Herve P, et al. Haemodynamic evaluation of pulmonary hypertension. *Eur Resp J* 2002; 20: 1314–1331.
5. Castelain V, Hervé P, Lecarpentier Y, et al. Pulmonary artery pulse pressure and wave reflection in chronic pulmonary thromboembolism and primary pulmonary hypertension. *J Am Coll Cardiol* 2001; 37: 1085–1092.
6. Su J, Manisty C, Parker KH, et al. Wave intensity analysis provides novel insights into pulmonary arterial hypertension and chronic thromboembolic pulmonary hypertension. *J Am Heart Assoc* 2017; 6: e006679.
7. Quail MA, Knight DS, Steeden JA, et al. Noninvasive pulmonary artery wave intensity analysis in pulmonary hypertension. *Am J Physiol Heart Circu Physiol* 2015; 308: H1603–H1611.
8. Frost A, Badesch D, Gibbs JSR, et al. Diagnosis of pulmonary hypertension. *Eur Resp J* 2019; 53: 1801904.
9. Kim NH, Delcroix M, Jenkins DP, et al. Chronic thromboembolic pulmonary hypertension. *J Am Coll Cardiol* 2013; 62: D92–D99.
10. Gude MJL, de la Sota EP, Gil AF, et al. Pulmonary thromboendarterectomy in 106 patients with chronic thromboembolic pulmonary hypertension. *Archivos de Bronconeumología (English Edition)* 2015; 51: 502–508.
11. Simonneau G, Torbicki A, Dorfmüller P, et al. The pathophysiology of chronic thromboembolic pulmonary hypertension. *Eur Resp Rev* 2017; 26: 160112.
12. Pepke-Zaba J, Jansa P, Kim NH, et al. Chronic thromboembolic pulmonary hypertension: role of medical therapy. *Eur Resp J* 2013; 41: 985–990.
13. Su J, Hughes AD, Simonsen U, et al. Impact of pulmonary endarterectomy on pulmonary arterial wave propagation and reservoir function. *Am J Physiol Heart Circ Physiol* 2019; 317: H505–H516.
14. Gerges C, Gerges M, Friewald R, et al. Microvascular disease in chronic thromboembolic pulmonary hypertension: hemodynamic phenotyping and histomorphometric assessment. *Circulation* 2020; 141: 376–386.
15. Kiely DG, Levin DL, Hassoun PM, et al. Statement on imaging and pulmonary hypertension from the Pulmonary Vascular Research Institute (PVRI). *Pulm Circ* 2019; 9: 2045894019841990.
16. Tawhai MH, Clark AR and Burrowes KS. Computational models of the pulmonary circulation: insights and the move towards clinically directed studies. *Pulm Circ* 2011; 1: 224–238.
17. Kheyfets VO, Rios L, Smith T, et al. Patient-specific computational modeling of blood flow in the pulmonary arterial circulation. *Comput Meth Program Biomed* 2015; 120: 88–101.
18. Clark AR, Tawhai MH, Hoffman EA, et al. The interdependent contributions of gravitational and structural features to perfusion distribution in a multiscale model of the pulmonary circulation. *J Appl Physiol* 2011; 110: 943–955.
19. Qureshi MU, Vaughan GD, Sainsbury C, et al. Numerical simulation of blood flow and pressure drop in the pulmonary arterial and venous circulation. *Biomech Model Mechanobiol* 2014; 13: 1137–1154.
20. Acosta S, Puelz C, Rivière B, et al. Cardiovascular mechanics in the early stages of pulmonary hypertension: a computational study. *Biomech Model Mechanobiol* 2017; 16: 2093–2112.
21. Wang Z and Chesler NC. Pulmonary vascular wall stiffness: an important contributor to the increased right ventricular afterload with pulmonary hypertension. *Pulm Circ* 2011; 1: 212–223.
22. Heath D and Edwards JE. The pathology of hypertensive pulmonary vascular disease: a description of six grades of structural changes in the pulmonary arteries with special reference to congenital cardiac septal defects. *Circulation* 1958; 18: 533–547.
23. Colebank MJ, Qureshi MU, Rajagopal S, et al. A multiscale model of vascular function in chronic thromboembolic pulmonary hypertension. *Am J Physiol Heart Circ Physiol* 2021; 321: H318–H338.
24. Qureshi MU and Hill NA. A computational study of pressure wave reflections in the pulmonary arteries. *J Math Biol* 2015; 71: 1525–1549.
25. Clark AR and Tawhai M. Temporal and spatial heterogeneity in pulmonary perfusion: a mathematical model to predict interactions between macro-and micro-vessels in health and disease. *ANZIAM J* 2018; 59: 562–580.
26. Burrowes KS, Hunter PJ and Tawhai MH. Anatomically based finite element models of the human pulmonary arterial and venous trees including supernumerary vessels. *J Appl Physiol* 2005; 99: 731–738.
27. Hoffman EA, Reinhardt JM, Sonka M, et al. Characterization of the interstitial lung diseases via density-based and texture-based analysis of computed tomography images of lung structure and function1. *Acad Radiol* 2003; 10: 1104–1118.
28. Osanlouy M, Clark AR, Kumar H, et al. Lung and fissure shape is associated with age in healthy never-smoking adults aged 20–90 years. *Scientif Rep* 2020; 10: 1–13.
29. Haefeli-Bleuer B and Weibel ER. Morphometry of the human pulmonary acinus. *Anat Rec* 1988; 220: 401–414.
30. Fung Y and Sobin S. Theory of sheet flow in lung alveoli. *J Appl Physiol* 1969; 26: 472–488.
31. Fung Y and Sobin S. Elasticity of the pulmonary alveolar sheet. *Circ Res* 1972; 30: 451–469.
32. Fung Y-C. Theoretical pulmonary microvascular impedance. *Ann Biomed Eng* 1972; 1: 221–245.
33. Duan B and Zamir M. Viscous damping in one-dimensional wave transmission. *J Acoust Soc Am* 1992; 92: 3358–3363.
34. Zhou Q, Gao J, Huang W, et al. Vascular impedance analysis in human pulmonary circulation. *Proceedings of IMECE ASME International Mechanical Engineering Congress and Exposition*, IMECE, 2002, pp.433–434.
35. Zhuang F, Fung Y and Yen R. Analysis of blood flow in cat's lung with detailed anatomical and elasticity data. *J Appl Physiol* 1983; 55: 1341–1348.

36. Clark A, Burrowes K and Tawhai M. The impact of microembolism size on haemodynamic changes in the pulmonary micro-circulation. *Resp Physiol Neurobiol* 2011; 175: 365–374.
37. Yen R, Fung Y and Bingham N. Elasticity of small pulmonary arteries in the cat. *J Biomech Eng* 1980; 102: 170–177.
38. Clark A, Milne D, Wilsher M, et al. Lack of functional information explains the poor performance of 'clot load scores' at predicting outcome in acute pulmonary embolism. *Resp Physiol Neurobiol* 2014; 190: 1–13.
39. Postles A, Clark AR and Tawhai MH. Dynamic blood flow and wall shear stress in pulmonary hypertensive disease. In: 2014 36th annual international conference of the IEEE engineering in medicine and biology society, 2014, pp.5671–5674. Piscataway, NJ: IEEE.
40. Moser KM and Bioor CM. Pulmonary vascular lesions occurring in patients with chronic major vessel thromboembolic pulmonary hypertension. *Chest* 1993; 103: 685–692.
41. Krenz GS and Dawson CA. Flow and pressure distributions in vascular networks consisting of distensible vessels. *Am J Physiol Heart Circ Physiol* 2003; 284: H2192–H2203.
42. Fung YC, Microcirculation. In: *Biodynamics-Circulation*. Springer, Verlag, New York, 1984, pp. 224–285.
43. Pries A, Secomb TW and Gaehtgens P. Biophysical aspects of blood flow in the microvasculature. *Cardiovasc Res* 1996; 32: 654–667.
44. Burrowes K, Clark A, Marcinkowski A, et al. Pulmonary embolism: predicting disease severity. *Philos Trans R Soc A* 2011; 369: 4255–4277.
45. Burrowes K, Clark A and Tawhai M. Blood flow redistribution and ventilation-perfusion mismatch during embolic pulmonary arterial occlusion. *Pulm Circ* 2011; 1: 365–376.
46. Burrowes K, Clark A, Wilsher M, et al. Hypoxic pulmonary vasoconstriction as a contributor to response in acute pulmonary embolism. *Ann Biomed Eng* 2014; 42: 1631–1643.
47. Pepke-Zaba J, Delcroix M, Lang I, et al. Chronic thromboembolic pulmonary hypertension (CTEPH) results from an international prospective registry. *Circulation* 2011; 124: 1973–1981.
48. Piene H. Pulmonary arterial impedance and right ventricular function. *Physiol Rev* 1986; 66: 606–652.
49. Haneda T, Nakajima T, Shirato K, et al. Effects of oxygen breathing on pulmonary vascular input impedance in patients with pulmonary hypertension. *Chest* 1983; 83: 520–527.
50. Kussmaul WG, Wieland JM and Laskey WK. Pressure-flow relations in the pulmonary artery during myocardial ischaemia: implications for right ventricular function in coronary disease. *Cardiovasc Res* 1988; 22: 627–638.
51. Milnor WR, Conti CR, Lewis KB, et al. Pulmonary arterial pulse wave velocity and impedance in man. *Circ Res* 1969; 25: 637–649.
52. Murgo JP and Westerhof N. Input impedance of the pulmonary arterial system in normal man. Effects of respiration and comparison to systemic impedance. *Circ Res* 1984; 54: 666–673.
53. Champion HC, Michelakis ED and Hassoun PM. Comprehensive invasive and noninvasive approach to the right ventricle–pulmonary circulation unit. *Circulation* 2009; 120: 992–1007.
54. Ebrahimi BS, Tawhai MH, Kumar H, et al. Wave reflection in an anatomical model of the pulmonary circulation in local and global hypertensive disease. In: 2019 41st annual international conference of the IEEE engineering in medicine and biology society (EMBC), 2019, pp.4973–4976. Piscataway, NJ: IEEE.
55. Karreman G. Some contributions to the mathematical biology of blood circulation. Reflections of pressure waves in the arterial system. *Bull Math Biophys* 1952; 14: 327–350.
56. Humbert M. Pulmonary arterial hypertension and chronic thromboembolic pulmonary hypertension: pathophysiology. *Eur Resp Rev* 2010; 19: 59–63.
57. Tuder RM, Abman SH, Braun T, et al. Development and pathology of pulmonary hypertension. *J Am Coll Cardiol* 2009; 54: S3–S9.
58. Egermayer P and Peacock A. Is pulmonary embolism a common cause of chronic pulmonary hypertension? Limitations of the embolic hypothesis. *Eur Resp J* 2000; 15: 440–448.
59. Peacock A, Simonneau G and Rubin L. Controversies, uncertainties and future research on the treatment of chronic thromboembolic pulmonary hypertension. *Proc Am Thorac Soc* 2006; 3: 608–614.
60. Simonneau G, Montani D, Celermajer DS, et al. Haemodynamic definitions and updated clinical classification of pulmonary hypertension. *Eur Resp J* 2019; 53: 1801913.
61. Madani MM, Auger WR, Pretorius V, et al. Pulmonary endarterectomy: recent changes in a single institution's experience of more than 2,700 patients. *Ann Thorac Surg* 2012; 94: 97–103.
62. Naeije R and Huez S. Right ventricular function in pulmonary hypertension: physiological concepts. *Eur Heart J Suppl* 2007; 9: H5–H9.
63. Lai Y-C, Potoka KC, Champion HC, et al. Pulmonary arterial hypertension: the clinical syndrome. *Circ Res* 2014; 115: 115–130.
64. Spruijt OA, Bogaard H-J and Vonk-Noordegraaf A. Pulmonary arterial hypertension combined with a high cardiac output state: three remarkable cases. *Pulm Circ* 2013; 3: 440–443.
65. Brogan TV, Mellema JD, Martin LD, et al. Spatial and temporal heterogeneity of regional pulmonary blood flow in piglets. *Pediatr Res* 2007; 62: 434–439.
66. Glenny R, Polissar N, McKinney S, et al. Temporal heterogeneity of regional pulmonary perfusion is spatially clustered. *J Appl Physiol* 1995; 79: 986–1001.
67. Glenny RW and Robertson HT. Fractal modeling of pulmonary blood flow heterogeneity. *J Appl Physiol* 1991; 70: 1024–1030.
68. Jones A, Hansell D and Evans T. Quantifying pulmonary perfusion in primary pulmonary hypertension using electron-beam computed tomography. *Eur Resp J* 2004; 23: 202–207.
69. Ussavarungsi K, Lee AS and Burger CD. Mosaic pattern of lung attenuation on chest CT in patients with pulmonary hypertension. *Diseases* 2015; 3: 205–212.
70. Kasai H, Tanabe N, Fujimoto K, et al. Mosaic attenuation pattern in non-contrast computed tomography for the assessment of pulmonary perfusion in chronic thromboembolic pulmonary hypertension. *Resp Investig* 2017; 55: 300–307.
71. Bernardo R, Vanderpool R and Rischard F. The pulmonary artery pulsatility index correlates with ventriculo-vascular

coupling and elevated filling pressures in patients with pulmonary arterial hypertension. *Eur Resp J* 2018; 52: PA3314.
72. Palecek T, Jansa P, Ambroz D, et al. Are pulmonary artery pulsatility indexes able to differentiate chronic pulmonary thromboembolism from pulmonary arterial hypertension? An echocardiographic and catheterization study. *Heart Vessels* 2011; 26: 176–182.
73. Ruiz-Cano MJ, Grignola J, Barberá JA, et al. The distribution of the obstruction in the pulmonary arteries modifies pulsatile right ventricular afterload in pulmonary hypertension. *Int J Cardiol* 2015; 181: 232–234.
74. Su J, Hilberg O, Howard L, et al. A review of wave mechanics in the pulmonary artery with an emphasis on wave intensity analysis. *Acta Physiol* 2016; 218: 239–249.
75. Zambanini A, Cunningham SL, Parker KH, et al. Wave-energy patterns in carotid, brachial, and radial arteries: a non-invasive approach using wave-intensity analysis. *Am J Physiol Heart Circ Physiol* 2005; 289: H270–H276.
76. Stacher E, Graham BB, Hunt JM, et al. Modern age pathology of pulmonary arterial hypertension. *Am J Resp Crit Care Med* 2012; 186: 261–272.
77. Clark AR, Burrowes KS and Tawhai MH. Contribution of serial and parallel microperfusion to spatial variability in pulmonary inter-and intra-acinar blood flow. *J Appl Physiol* 2010; 108: 1116–1126.
78. Kim HJ, Vignon-Clementel IE, Figueroa CA, et al. On coupling a lumped parameter heart model and a three-dimensional finite element aorta model. *Ann Biomed Eng* 2009; 37: 2153–2169.
79. Le Rolle V, Hernandez AI, Richard P-Y, et al. A bond graph model of the cardiovascular system. *Acta Biotheor* 2005; 53: 295–312.

Notation

Y_c	Characteristic admittance
c_0	Characteristic wave velocity
r_0	Unstrained vessel radius
r	Vessel radius
α_0	Vascular wall compliance
α_c	Capillary wall compliance
α_h	Compliance reduction factor due to hypertrophy and hyperplasia
α_f	Compliance reduction factor due to fibrosis
ω	Frequency
μ	Blood viscosity
ρ	Blood density
Y_e	Effective admittance
q_0	Incident flow waveform
ω_n	nth harmonic frequency
Φ_n	nth phase offset
E	Young modulus
P_{tm}	Transmural pressure
H_0	Unstrained capillary sheet thickness
H	Capillary sheet thickness
h	Thickness of the vessel wall
F	Friction factor constant
k	Friction factor constant
L_c	Average length of a capillary unit
μ_c	Apparent blood viscosity in capillaries
p_f	Pruning factor
n_f	Narrowing factor due to proliferation of intima